Cement and Concrete Research 144 (2021) 106438

Contents lists available at ScienceDirect

Cement and Concrete Research

journal homepage: www.elsevier.com/locate/cemconres

The effect of equilibration time on Al uptake in C-S-H

Sonya Barzgar [a,b,*], Mohamed Tarik [c], Christian Ludwig [b,c], Barbara Lothenbach [a,d]

[a] Empa, Concrete & Asphalt Laboratory, CH-8610 Dübendorf, Switzerland
[b] École Polytechnique Fédéral de Lausanne (EPFL), ENAC IIE GR-LUD, CH-1015 Lausanne, Switzerland
[c] Paul Scherrer Institute (PSI), ENE LBK CPM, 5232 Villigen PSI, Switzerland
[d] NTNU, Department of Structural Engineering, Trondheim, Norway

ARTICLE INFO

Keywords:
C-A-S-H
Equilibration time
ICP-OES
TGA
FTIR

ABSTRACT

Calcium silicate hydrate (C-S-H) is the main hydration product of Portland cements. The partial replacement of Portland cements by supplementary cementitious materials can result in C-S-H with lower Ca/Si ratios and more aluminum and alkalis. The effect of equilibration time on Al uptake in C-S-H was investigated using equilibration times from 7 days up to 3 years. Lower Al concentrations were measured in the solution after longer equilibration times. In addition, a higher uptake of Al in C-S-H was observed based on the decrease in the content of secondary phases. Little further decrease in Al concentrations was observed after 2 years and longer at low Ca/Si. At high Ca/Si no significant change in solution concentrations was observed after more than 3 month, while the destabilization of secondary phases continued up to 1 year, indicating that a (meta)stable equilibrium was reached faster at higher Ca/Si ratios.

1. Introduction

Calcium silicate hydrate (C-S-H) is the main hydration product of Portland cements (PC) and contributes significantly to compressive strength and other mechanical properties of cement based materials [1–3]. In order to reduce the CO_2 emissions from cement production, the PC can partially be replaced by supplementary cementitious materials (SCM) such as blast furnace slags, by-products from steel production, fly ash from coal combustion, or calcined clays [2–6]. The reaction of PC with SCM with high Si and Al contents changes the composition of C-S-H with lowering the Ca/Si ratio and increasing the Al/Si ratio [3,7,8]. This can be relevant for the long-term stability of construction materials [9] as well as for oil well cement or stabilized filter ashes [10,11].

The incorporation of Al in the C-S-H structure leads to the formation of so-called calcium alumino silicate hydrate (C-A-S-H) phases, i.e. C-S-H containing aluminum [12,13]. C-A-S-H phases consist of a calcium oxide polyhedral layers flanked with “dreierketten” – tetrahedral (alumino) silicate chains – on both sides and water as well as counter-ions (e.g., Ca^{2+} and OH^-) in an interlayer between two such layers [14–17]. Two of these silica tetrahedra are linked to the calcium oxide layer and called pairing tetrahedra, while the third one, the bridging tetrahedron, links the two pairing tetrahedra [15,16,18]. The interlayer containing water, calcium, alkalis and other ions connects a number of sheets together. The silica chain length varies with the Ca/Si ratio. At high Ca/Si ratios, the silica tetrahedral chains are short [16,19,20]. However, at Ca/Si ratios in the range of 0.6–0.8, long silicate tetrahedral chains occur, in which repeating units of one bridging site is connected to two paired silicate tetrahedral sites on either side [16,18,21,22]. The incorporation of Al as tetrahedral AlO_4 occurs into the bridging sites of silica tetrahedral chains in which four-fold coordinated Al (Al^{IV}) is the dominant environment at low Ca/Si ratios [23], however, at high Ca/Si ratios five-fold coordinated Al (Al^{V}) and six-fold coordinated Al (Al^{VI}) are also present [24].

The data available in the literature point towards a possible dependency of C-S-H solubility [22] and of aluminum uptake on the reaction time [7,12,20,25,26]. The solubility of C-S-H has been observed to depend also on the synthesis methods, indicating the possible existence of several metastable C-S-H phases after short equilibration times [22]. The incorporation of Al in C-S-H investigated after 1 day equilibration for C-A-S-H with a Ca/Si = 0.66 [27] and 5 days equilibration for C-A-S-H with Ca/Si ratios of 0.7 and 0.95 [26] showed a linear increase of Al uptake in C-S-H with the amount of Al present. No precipitation of secondary phases such as strätlingite ($2CaO.Al_2O_3.SiO_2.8H_2O$), katoite ($3CaO.Al_2O_3.6H_2O$) and microcrystalline aluminum hydroxide ($Al(OH)_3$) was reported [26,27]. After equilibration times of 6 months and longer, in addition to C-A-S-H also the precipitation of strätlingite,

* Corresponding author at: Empa, Concrete & Asphalt Laboratory, CH-8610 Dübendorf, Switzerland.
E-mail address: sonya.barzgar@empa.ch (S. Barzgar).

https://doi.org/10.1016/j.cemconres.2021.106438
Received 16 December 2020; Received in revised form 5 March 2021; Accepted 14 March 2021
Available online 31 March 2021

katoite and $Al(OH)_3$ has been observed in other studies, which lowered the aluminum concentration in the aqueous solution and thus increased the Al uptake in C-S-H [16,20,28]. Further analysis revealed that the content of katoite, which had precipitated in the first months in addition to C-A-S-H phases, decreased with equilibration time, indicating an increasing Al uptake in C-S-H with time [12] pointing towards a continuing restructuring of C-A-S-H.

The main aim of this study was to investigate the effect of different reaction times on Al uptake in C-S-H. Long- and short-term sorption isotherms were recorded in order to perform a kinetic study at different ages of C-A-S-H samples. C-A-S-H samples were synthesized using different Ca/Si ratios, Al/Si ratios and at different alkali hydroxide concentrations. Samples were filtrated after different equilibration times from 7 days to 56 days in short-term experiments and from 3 months to 3 years in long-term experiments. The elemental concentrations of different ions in the solution were determined by Inductively Coupled Plasma Optical Emission Spectrometry (ICP-OES).

2. Material and methods

Short- and long-term sorption experiments were performed in order to investigate the effect of different equilibration times on Al uptake in C-S-H. In long-term experiments, the synthesis of samples were performed at room temperature by following the same procedure as detailed in [29] by adding a total of 3.8 g calcium oxide (CaO), silica fume (SiO_2, Aerosil 200, Evonik) and calcium aluminate (CA: $CaO{\cdot}Al_2O_3$) into 171 mL of Milli-Q water or NaOH solutions (liquid/solid = 45 mL/g) to obtain C-A-S-H with different compositions (Table 1). CaO was obtained by burning calcium carbonate ($CaCO_3$, Merck, pro analysis) at 1000 °C for 12 h. CA was synthesized by heating the mixture of $CaCO_3$ and Al_2O_3 (Sigma Aldrich) at 800 °C for 1 h, at 1000 °C for 4 h and at 1400 °C for 8 h. Then, the mixture was cooled down with a rate of 600 °C/h. The molar ratios of CaO, SiO_2 and CA were varied in order to obtain C-A-S-H with Ca/Si ranging from 0.6 to 1.4, and Al/Si from 0 to 0.1, as indicated in Table 1. In addition, NaOH concentrations of 0, 0.1, 0.5 and 1 M were selected to cover the range of pH values relevant for hydrated cements [20].

In the short-term experiments, C-S-H samples with Ca/Si ratios of 0.8 and 1.2 and 1 M NaOH were synthesized and equilibrated for 1 month. Afterwards, 0.086 and 0.073 g of sodium aluminate ($NaAlO_2$), corresponding to an Al/Si molar ratio of 0.03 and 1000 mM Na, were added to the pre-equilibrated C-S-H samples with Ca/Si ratios of 0.8 and 1.2, respectively. The composition of liquid and solid phases of C-S-H samples containing Al (C-A-S-H) was measured after 7, 14, 28 and 56 days.

All samples were synthesized in a nitrogen filled glovebox to minimize carbonation and were stored in 200 mL PE-HD containers placed on a horizontal shaker moving at 100 rpm and equilibrated at 20 °C. After different equilibration times, the solid and liquid phases were separated by vacuum filtration using nylon filters (pore size: 0.45 μm) and analyzed.

Table 1
The Ca/Si, Al/Si molar ratios and NaOH concentrations used to prepare C-A-S-H at 20 °C. (note: the samples were prepared at each combination of Ca/Si, Al/Si and NaOH concentration with 4 replicates in order to be analyzed after different equilibration times). (*: samples at Ca/Si ratio of 0.8 were analyzed also after 24 and 36 months).

Experiment	Ca/Si	Al/Si	NaOH (mol/L)	Equilibration time
Short-term	0.8 and 1.2	0.03	1	7, 14, 28, 56 days
Long-term	0.6, 0.8*, 1.0, 1.2 and 1.4	0 0.001 0.003 0.01 0.03 0.05 0.1	0, 0.1, 0.5, 1	3 and 12 months*

2.1. Solution phase analysis

ICP-OES was used to measure the elemental concentrations of Na, Ca, Si and Al in the filtrates. The samples were first acidified with HNO_3 to have 1% HNO_3 (using Suprapur HNO_3, Merck). In order to keep the Na concentrations below 1100 mg/L for the ICP-OES analysis, the samples were diluted with 1% HNO_3. Multi-standard solutions and blank solution (1% HNO_3), containing Al, Ca and Si, were prepared in the range from 0 to 20 mg/L (0, 0.2, 2 and 20) for ICP-OES.

The pH measurements were made at room temperature with a Knick pH meter (pH-Meter 766) equipped with a Knick SE100 electrode to measure the hydroxide concentration (OH^-) on the undiluted samples on the day of the filtration. The pH electrode was calibrated against 0.1, 0.2, 0.5 and 1 M NaOH solutions in order to minimize the alkali error [30].

2.2. Solid phase analysis

In order to investigate the effect of equilibration time on the composition of the solid phase, analysis were performed using Thermogravimetric Analysis (TGA), X-Ray Diffraction (XRD) and Fourier-Transform Infrared Spectroscopy (FTIR). Prior to analysis, the filtrated samples were washed first with a 50%–50% (volumetric) water-ethanol solution and then with 94% ethanol inside the glovebox to avoid the precipitation of alkali compounds during drying and to remove the free water, respectively. The samples were then dried in the freeze dryer for one week and then stored until analysis (at least 1 week) in nitrogen filled desiccators in the presence of saturated $CaCl_2.2H_2O$ solution, which generates a relative humidity of 30%, following the procedure described by [25,28].

TGA data were acquired using a TGA/SDTA851e Mettler Toledo device. The weight loss of approximately 30 mg of each sample was recorded under N_2 atmosphere from 30 °C up to 980 °C with a heating rate of 20 °C/min. The water loss of strätlingite, $Al(OH)_3$, katoite, portlandite and $CaCO_3$ was quantified using the tangential method and the theoretical weight loss of solids based on the measured weight loss between 150–240, 240–300, 300–350, 350–450 and 600–800 °C, respectively [31], was used to calculate the amount of these solids.

The X-ray powder diffraction patterns were recorded using the PANalycatical X'Pert Pro MDF diffractometer equipped with an X'Celerator detector. The diffraction patterns were collected in increments of 5° to 55° 2θ at a conventional step size of 0.026° 2θ and a step measurement time of 447 s. The presence of different phases was determined with X'Pert HighScore Plus.

FTIR spectra were recorded in the range of 400–4300 cm^{-1} on a Bruker Tensor 27 spectrometer with a resolution of 4 cm^{-1} by transmittance on small amounts of powder. To make the comparison easier, the spectra were corrected for background and scaled to the maximum signal of Si—O bonds at 1100 cm^{-1}. The second derivative of the measured transmittance (T) over the wavelength (W): d^2T/dW^2, were also plotted in order to better identify the different bands and differentiate the wavenumbers [32].

The elemental composition in C-A-S-H was calculated by mass balance taking into account the initial quantities, the amount of Al, Ca, Si and Na in secondary phases, if present and the fraction of Al, Ca, Si and Na in solution as detailed in [29].

2.3. Thermodynamic modeling

Thermodynamic modeling was performed with Gibbs Free Energy Minimization (GEM-Selektor) software [33,34], version 3.7. The PSI-Nagra thermodynamic database [35] was used to obtain the thermodynamic data for aqueous species, portlandite and amorphous SiO_2. The

solubility of microcrystalline $Al(OH)_3$, strätlingite, C-S-H and katoite was taken from the Cemdata18 database [36] and the data for the zeolitic phases such as Ca-gismondine ($CaAl_2Si_2O_8$ $4.5H_2O$) and OH-sodalite ($Ca_8Al_6Si_6O_{24}(OH)_2$ $2H_2O$) from [37]. The CSHQ thermodynamic solid solution model was used in order to model the concentrations in the C-S-H system [33]. The activity coefficients of the aqueous species γ_i were calculated using the extended Debye-Hückel equation (Eq. (1)) with common ion-size parameter $a_i = 3.31$ Å for NaOH solutions [38] and common third parameter b_y according to

$$log\gamma_i = \frac{-A_y z_i^2 \sqrt{I}}{1 + B_y a_i \sqrt{I}} + b_y I \quad (1)$$

where z_i denotes the charge of species i, I the effective molal ionic strength, b_y is a semi-empirical parameter (~0.098 for NaOH electrolyte at 25 °C), and A_y and B_y are P, T-dependent coefficients. This activity correction is applicable up to ~1 M ionic strength [39].

Solubility products (K_{so}) for C-A-S-H were calculated from the generalized dissolution reaction shown in Eq. (2):

$$(CaO)_a\,(SiO_2)_b\,(Al_2O_3)_c\,(H_2O)_{d(s)} \underset{\rightleftarrows}{K_{so}} a{Ca^{2+}}_{(aq)} + b{HSiO_3}^-_{(aq)} + 2c{AlO_2}^-_{(aq)} + (2a - b - 2c){OH^-}_{(aq)} + (c + d - a)\,{H_2O}_{(l)} \quad (2)$$

where a, b, c and d are the respective stoichiometric coefficients for CaO, SiO_2, Al_2O_3 and H_2O in C-A-S-H. This reaction implies the following relationship for K_{so} for Ca/Si = 0.8 (Eq. (3)):

$$K_{so} = \{{Ca^{2+}}_{(aq)}\}^{0.777} \cdot \{{HSiO_3}^-_{(aq)}\}^{0.971} \cdot \{{AlO_2}^-_{(aq)}\}^{0.029} \cdot \{{OH^-}_{(aq)}\}^{0.554} \cdot \{{H_2O}_{(l)}\}^{1.02} \quad (3)$$

And for Ca/Si = 1.2 (Eq. (4)):

$$K_{so} = \{{Ca^{2*}}_{(aq)}\}^{1.165} \cdot \{{HSiO_3}^-_{(aq)}\}^{0.971} \cdot \{{AlO_2}^-_{(aq)}\}^{0.029} \cdot \{{OH^-}_{(aq)}\}^{1.33} \cdot \{{H_2O}_{(l)}\}^{1.19} \quad (4)$$

Activities of ${Ca^{2+}}_{(aq)}$, ${HSiO_3}^-_{(aq)}$, ${AlO_2}^-_{(aq)}$, ${OH^-}_{(aq)}$ and ${H_2O}_{(l)}$ species were calculated with GEM-Selektor v3.7 using the measured concentrations of Ca, Si, Al and OH^- in the supernatants.

The saturation index (SI) of different solids according to SI=log *IAP*/K_{so} was calculated using the elemental concentrations of Al, Ca, Si and Na. The ion activity product (*IAP*) was calculated based on the measured concentrations in solution. A positive saturation index (> 0) indicates that the solution is oversaturated with respect to this solid phase and that this phase could possibly precipitate. A negative value indicates undersaturation. The SI calculation was used to verify the solid phase composition found experimentally.

3. Results and discussion

3.1. The effect of time on solid phase

3.1.1. The effect of equilibration time on secondary phases

The changes in the water content of C-A-S-H and the possible presence of secondary phases with time are followed by TGA. The TGA analysis of C-A-S-H samples after different equilibration times of 7 days up to 3 years are shown in Fig. 1. The water present at the surface and interlayer of C-S-H is lost over a broad temperature range up to 150 °C in agreement with different studies on C-S-H [28,40]. An additional weight loss is observed for the samples after 7, 14, 28 and 56 days at ≈430 °C, although no crystalline phases have been observed to be present by XRD after 3 months [29]. This weight loss has been observed previously for C-S-H in the presence of Na and Al and was tentatively assigned to an unidentified calcium sodium aluminate silicate hydrate (C-N-A-S-H) [25]. This poorly defined weight loss is absent after 2 and 3 years of equilibration and no other solids were detected by TGA and XRD [29].

The physically bound water content of C-S-H is strongly dependent on the drying procedure, duration and the relative humidity [41], resulting in some variation of the total weight loss up to 600 °C as shown in Fig. 1. Based on the TGA data the H_2O/Si ratios have been calculated and compiled in Supplementary Information A. Despite some variation of the data, the H_2O/Si ratios are around 1.05 ± 0.15 for equilibration times from 7 days up to 2 years, however, a bit lower (0.85) after 3 years equilibration.

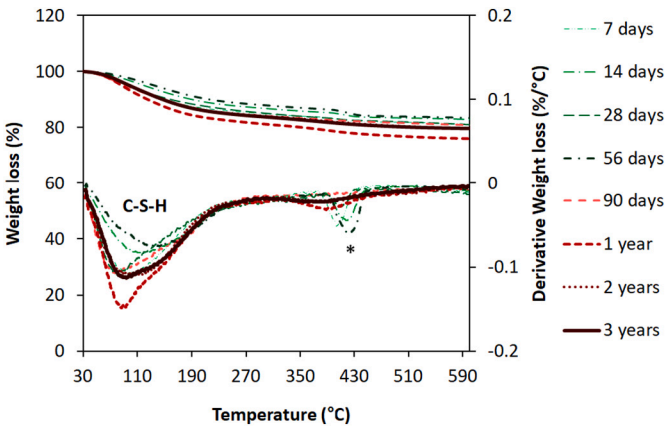

Fig. 1. The TGA of C-A-S-H after different equilibration times for Ca/Si = 0.8 and 1 M NaOH. (* signals assigned to an unidentified calcium sodium aluminate silicate hydrate (C-N-A-S-H) phase [25]).

The presence of Al could also lead to the formation of secondary phases containing Al. Microcrystalline $Al(OH)_3$ and strätlingite are observed by TGA mainly at low Ca/Si ratios and in the absence of NaOH, katoite mainly at higher Al contents but at all Ca/Si ratios and pH values (Supplementary Information A). In addition, the formation of zeolites or zeolitic precursor like Ca-gismondine and sodalite cannot be excluded at low Ca/Si ratios and high NaOH concentrations, although they are not clearly observed by TGA or XRD, as at Ca/Si = 0.6 some solutions are moderately oversaturated with respect to sodalite and at Ca/Si = 0.8 with respect to gismondine (Supplementary Information C). The TGA signal of the samples without alkali at Ca/Si ratio of 0.8 is also shown in Fig. 2a and b and at Ca/Si = 1.4 in Fig. 2c. While no or very little secondary phases are observed at Al/Si of 0.03 or lower, secondary phases are observed at higher Al/Si ratios in agreement with the observations of L'Hopital et al. [7]. Fig. 2 shows that increasing the equilibration time from 3 months to 3 years for samples with Al/Si = 0.1 and 0.2 leads to a decrease in the amount of secondary phases such as strätlingite, aluminum hydroxide and katoite. At Ca/Si = 0.8 and Al/Si ratio = 0.1, 1.4 wt% katoite is observed after 3 months equilibration which decreases to a non-detectable level after 3 years, while the solution remains undersaturated. Similarly at Al/Si = 0.2, increasing the equilibration time from 3 months to 3 years leads also to a decrease in the amount of $Al(OH)_3$ (from 1.4 wt% to 0.29 wt%) and katoite (from 2.1 wt% to 0.18 wt%) (Fig. 2b). An increase in equilibration time from 1 year to 3 years at Al/Si = 0.2 decreases the amount of strätlingite from 0.58 wt% to a non-detectable level. Also at Ca/Si ratio of 1.4 (Fig. 2c) the amount of katoite decreases from 1.9 wt% after 3 months to a non-detectable level after 1 year (around 0.28 wt%).

The XRD pattern of C-A-S-H samples at Ca/Si = 0.8 and Al/Si = 0.1 in the absence of NaOH is shown in Fig. 3. A trace of strätlingite and Al $(OH)_3$ is observed only after 3 months equilibration. In addition, the presence of katoite is observed after 3 months and 1 year equilibration, however, it disappears after 2 and 3 years. The decrease in the quantity of katoite with time is in agreement with TGA results as shown in Fig. 2a. L'Hopital et al. also observed katoite in addition to C-A-S-H phases after 6 months equilibration and suggested that katoite has formed initially from strongly oversaturated solutions and its quantity decreased with time for C-A-S-H at Al/Si = 0.1 as the solution was undersaturated with respect to katoite at the time studied [12]. The SI, in Supplementary

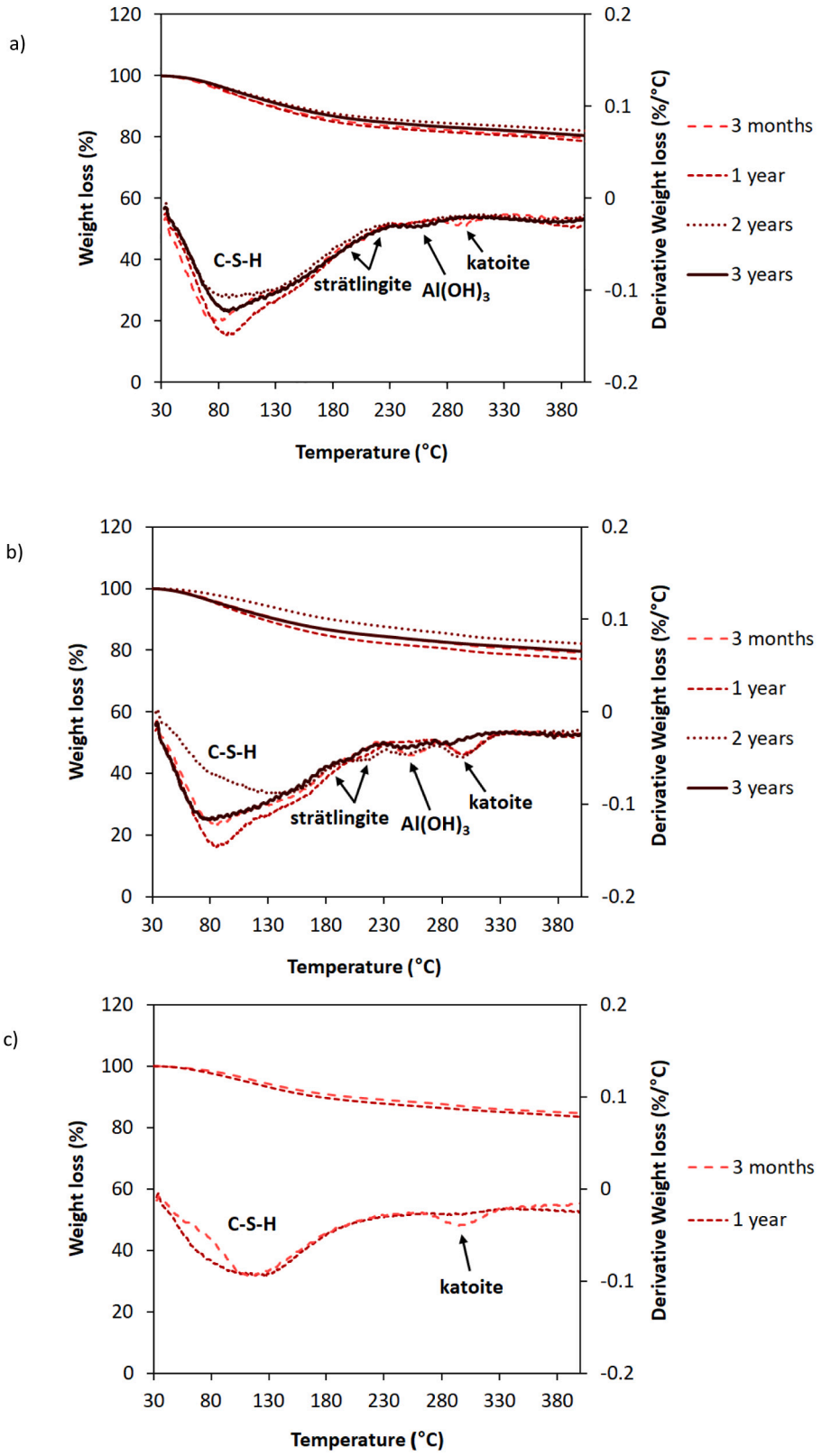

Fig. 2. The effect of equilibration time on the composition of secondary phases for a) Ca/Si = 0.8 & Al/Si = 0.1; b) Ca/Si = 0.8 & Al/Si = 0.2 and c) Ca/Si = 1.4 & Al/Si = 0.1 in the absence of NaOH.

Information C, also show more negative values for strätlingite, $Al(OH)_3$ and katoite with an increase in time. The SI values for a same Ca/Si and Al/Si ratio decrease with increasing the equilibration time, which is consistent with a decrease in the content of secondary phases. For example, for samples without alkali for Ca/Si ratio of 0.8 the SI values for $Al(OH)_3$ decrease from −0.6 to −1.8 and from −0.5 to −1.8 when moving from 3 months to 1 year equilibration for Al/Si ratios of 0.1 and 0.2, respectively. The observed destabilization of $Al(OH)_3$, strätlingite

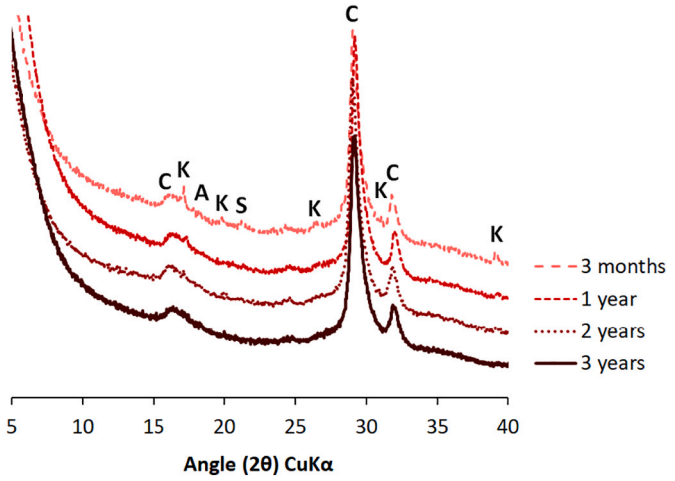

Fig. 3. The XRD pattern of C-A-S-H as a function of equilibration time in the absence of NaOH for Ca/Si = 0.8 and Al/Si = 0.1 (C: C-A-S-H, K: katoite, A: Al $(OH)_3$, S: strätlingite).

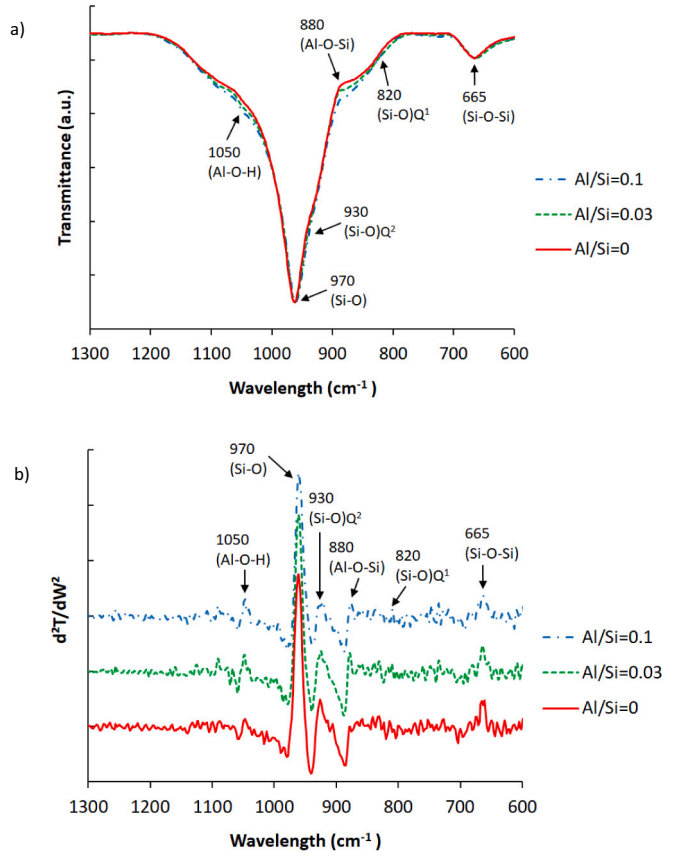

Fig. 4. The FTIR spectra for C-A-S-H samples without alkali at Ca/Si = 0.8 for 2 years equilibration and different Al/Si ratios: a) transmittance (T) vs. wavelength (W) and b) 2nd derivative of the transmittance d^2T/dW^2 vs. wavelength.

and katoite with time as reported in [7,12] and in the present paper, indicates consistently an increased uptake of aluminum in a thermodynamically more stable C-A-S-H phase with time.

3.1.2. The effect of equilibration time on the structure of C-A-S-H

The changes in the structure of C-A-S-H are investigated by FTIR for the samples with Ca/Si ratios of 0.8 and 1.2. All the FTIR spectra show absorption bands at 1300–850 cm^{-1}, which are typical for

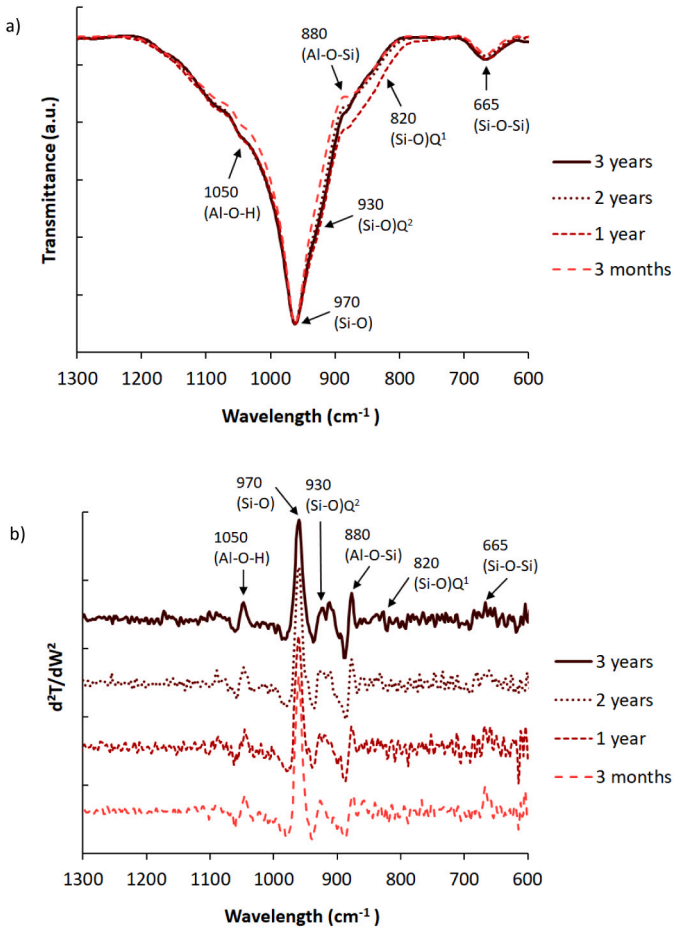

Fig. 5. The FTIR spectra for C-A-S-H samples without alkali at Ca/Si = 0.8 and Al/Si = 0.2 after different equilibration times: a) transmittance (T) vs. wavelength (W) and b) 2nd derivative of the transmittance d^2T/dW^2 vs. wavelength.

aluminosilicates and assigned to the asymmetric and symmetric stretching vibration of Si-O-Si and Si-O-Al bonds in $[SiO_4]^{4-}$ and $[AlO_4]^{5-}$ [42–44]. The signal observed at around 665 cm^{-1} is assigned to Si-O-Si bending vibrations and water librations and shows little variations with Ca/Si [45–50]. The signal at 820 cm^{-1} is related to Si—O stretching of Q^1 tetrahedra and is more intense at high Ca/Si ratios. The main signal ranging from 900 to 1200 cm^{-1} is assigned to the stretching and deformation or bending vibration of the Si—O bands [51]. The band centered in the range 950–970 cm^{-1} has often been attributed to Q^2 silica units of C-S-H [50,52,53]. However, a recent publication highlighted that the several bands contribute to that band at around 970 cm^{-1} [51]. Two bands at ~930 cm^{-1} and ~1060 cm^{-1} are associated with Q^2-silicate species, and a third band at ~1005 cm^{-1} is attributed to Q^1-silicate species [51]. This is in agreement with the observation of Yu et al. [50], where a higher intensity of shoulder above 1000 cm^{-1} was established at higher Ca/Si ratios. Bands in the range of 500–750 cm^{-1} can be assigned to the stretching vibrations of Al—O bonds of the octahedrally coordinated Al, and bands in the range of 750–900 cm^{-1} to the vibrations of Al—O bond in AlO_4 units [54]. The band at about 880 cm^{-1} has been associated with the stretching vibration of Al-O-Si (terminal bond) [55]. The symmetric bending of Al-O-H have been reported in the range of 1034–1075 cm^{-1} [58–60].

Fig. 4 shows the FTIR spectra for samples with Ca/Si ratio of 0.8 with no Al and with 0.03 and 0.1 Al/Si. The intensity of the shoulders at 880 cm^{-1} and 1050 cm^{-1} increases with increasing Al/Si ratios indicating the presence of more Al in C-S-H by increasing Al contents in the samples. Moreover, the intensity of the shoulder for Si—O stretching

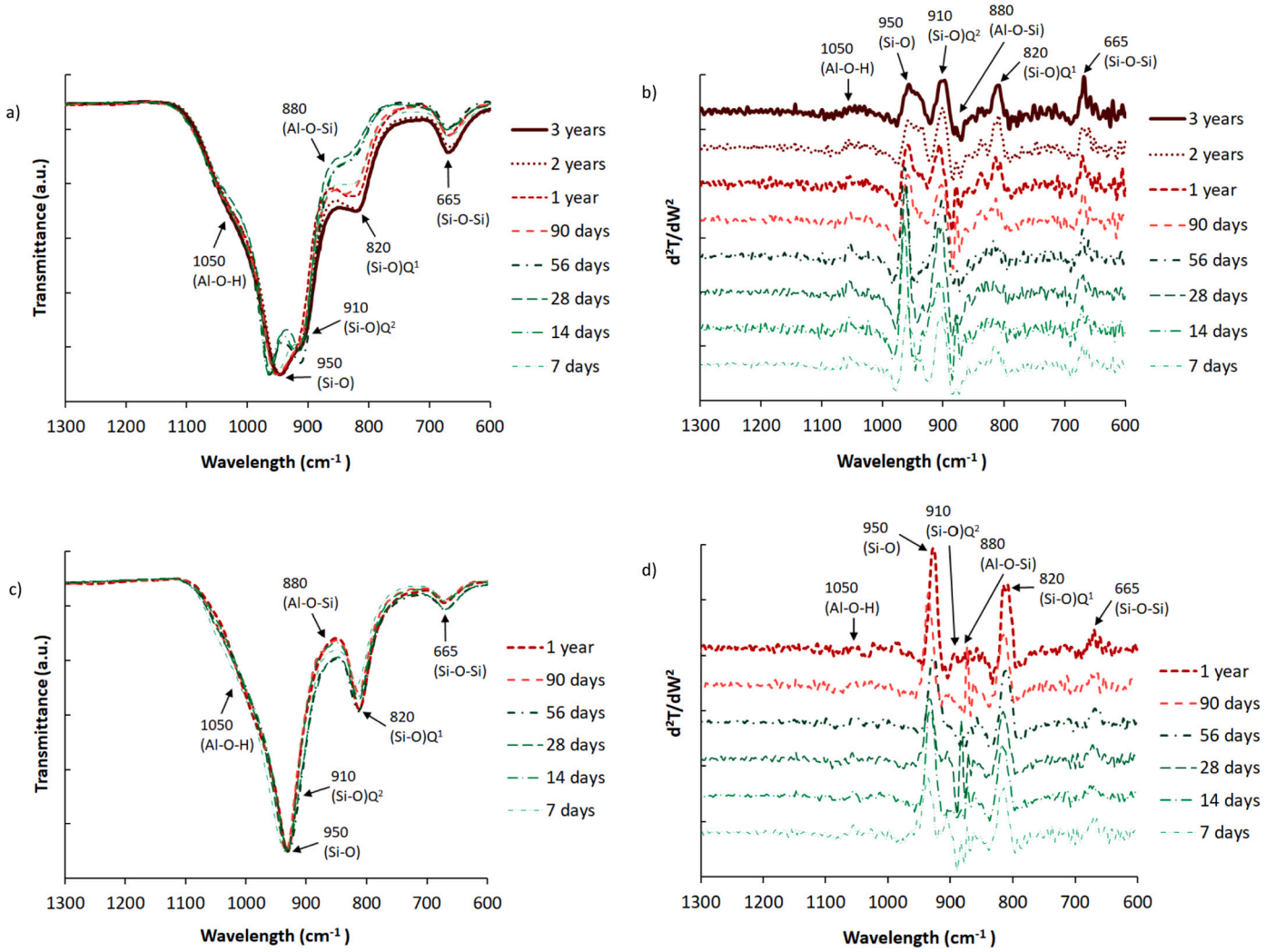

Fig. 6. The FTIR spectra for C-A-S-H samples in the presence of 1 M NaOH for Al/Si = 0.03 and different equilibration times: a) transmittance (T) vs. wavelength (W) for Ca/Si = 0.8; b) 2nd derivative of the transmittance d^2T/dW^2 vs. wavelength for Ca/Si = 0.8; c) transmittance vs. wavelength for Ca/Si = 1.2 and d) 2nd derivative of the transmittance d^2T/dW^2 vs. wavelength for Ca/Si = 1.2.

vibration of Q^2 sites at 930 cm^{-1} increases with increasing Al content, as is visible in Fig. 4a, which could be related to the replacement of silica in the Q^2 sites by Al.

The effect of equilibration time on C-A-S-H composition is represented in Fig. 5 for samples without alkali for Ca/Si ratio of 0.8 and Al/Si ratio of 0.2. The main difference is observed in the intensity of the Al-O-H shoulder at around 1050 cm^{-1} which increases with longer equilibration time indicating a rearrangement of the Al over time (Fig. 5a). Moreover, the intensity of Si—O stretching of Q^2 sites at 930 cm^{-1} increases with equilibration time, which could indicate longer silica chains with time. No clear changes are observed in the intensities of the other signals.

Fig. 6 shows the effect of equilibration time on C-A-S-H in the presence of 1 M NaOH for Ca/Si ratios of a, b) 0.8 and c, d) 1.2. At Ca/Si of 0.8, the intensity of (Si—O) Q^1 peak at 820 cm^{-1} is higher than in the alkali free samples (Fig. 5) indicating the presence of more end-of-chain-SiO_2 groups and thus shorter silica chain length in the presence of high alkali hydroxide concentrations, in agreement with Si-Nuclear Magnetic Resonance (NMR) observations of similar samples [20,25,61]. At Ca/Si of 1.2, the intensity of the band at 820 cm^{-1} is higher, consistent with the shorter silica chain length expected at higher Ca/Si ratios. For both Ca/Si ratios of 0.8 and 1.2, the intensity of (Si—O) Q^1 peak at 820 cm^{-1} increases with an increase in equilibration time. At Ca/Si = 0.8, the signal of Si—O stretching vibration at around 950 cm^{-1} shows a splitting into two signals at low equilibration times up to 56 days, while at later times only one signal is observed. Such a splitting of the signal can indicate a low symmetry [62]. When structural sites are present as groups of nonequivalent sites, it results in a splitting of the absorption bands indicating a low symmetry. The disappearance of this signal splitting indicates that environment becomes more symmetric with time, which suggests a structural rearrangement in the C-A-S-H at least up to 90 days. The Si—O stretching vibrations around 950 cm^{-1} and 910 cm^{-1} move to a lower wavelength with time for Ca/Si ratio of 0.8 and 1.2, respectively. Also, the intensity of the signal at around 665 cm^{-1}, which is related to the Si-O-Si vibrations and water librations [50], decreases with time which could indicate a restructuring of the water with time in the C-A-S-H structure. Less clear changes are observed at Ca/Si = 1.2, indicating that less rearrangement occurs at a higher Ca/Si ratio which is consistent with the observations in the liquid phase as discussed in Section 3.2.2.

3.2. The effect of time on aqueous concentrations and Al uptake

3.2.1. The effect of short and long equilibration times on C-A-S-H

The effect of equilibration time on Al uptake in C-S-H for Ca/Si ratios of 0.8 and 1.2 for samples containing 1 M NaOH is shown in Fig. 7. For

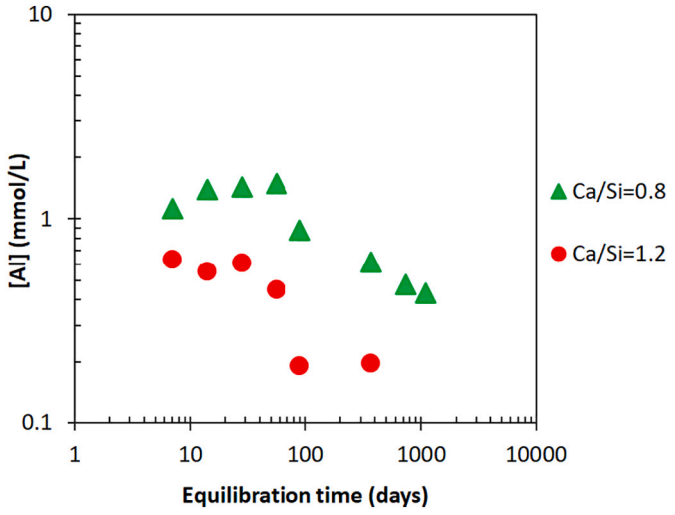

Fig. 7. The effect of equilibration time on the Al concentrations in solution for Ca/Si ratios of 0.8 and 1.2 in the presence of 1 M NaOH.

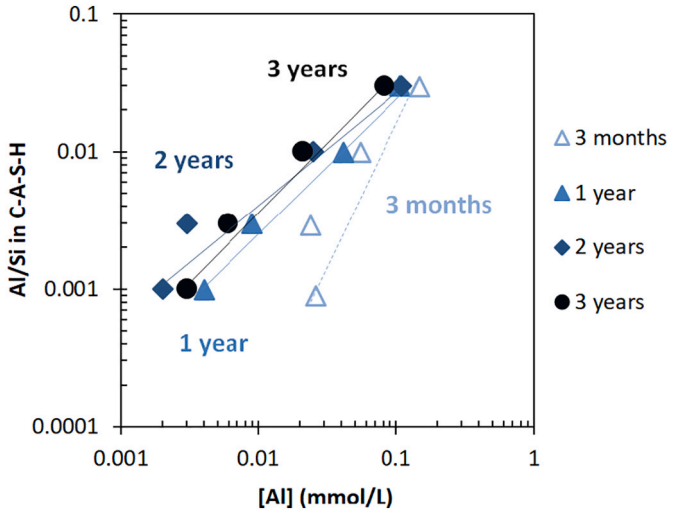

Fig. 8. The Al sorption isotherm on C-A-S-H for Ca/Si = 0.8 and 0.1 M NaOH recorded after different equilibration times. The darkness of colors indicates an increase in equilibration time; 3 months indicated by the lightest and 3 years represented by the darkest symbols. The lines serve as eye-guides only.

both Ca/Si ratio of 0.8 and 1.2 the Al concentrations seem quite constant between 7 and 28 days, but decrease clearly after 56 days, i.e. at the time when the FTIR signals indicate a clear structural rearrangement as shown in Fig. 6. This indicates an increase in Al uptake in C-S-H over time at both Ca/Si ratios. Little further change in Al concentration is observed at Ca/Si = 1.2 between 3 months and 1 year equilibration time indicating that a (meta)stable equilibrium might have been reached. In contrast, for Ca/Si = 0.8 the Al concentrations in solution continue to decrease, albeit more slowly, up to 3 years equilibration, indicating that equilibrium is reached slower at low Ca/Si than at high Ca/Si ratios.

This very slow ripening at low Ca/Si is visible in the presence of 0.1 M NaOH as shown in Fig. 8, where the Al uptake in C-S-H for the Ca/Si ratio of 0.8 is plotted from 3 months to 3 years (data for 0.5 and 1 M NaOH are shown in Supplementary Information D). In agreement with results discussed above, the decrease of Al concentrations and hence the uptake of Al in C-S-H accelerate over time. Increasing the equilibration time from 3 months to 1 year leads to a more distinct lowering of Al concentrations compared to the change from 1 year to 2 years. In fact, little changes in the Al concentrations are observed between 2 and 3 years equilibration indicating that the reaction of Al with C-S-H is approaching a metastable equilibrium after 2 years.

3.2.2. *The effect of Ca/Si, NaOH and time on Al uptake in C-S-H*

Fig. 9 shows the effect of equilibration time on the Al uptake in C-S-H at 5 different Ca/Si ratios of a) 0.6; b) 0.8; c) 1.0; d) 1.2 and e) 1.4. It can be seen (Fig. 9a-c) that at Ca/Si ratios of 0.6, 0.8 and 1.0 the aluminum concentrations decrease significantly with increasing the equilibration time from 3 months to 1 year. However, at higher Ca/Si ratios of 1.2 and 1.4 (Fig. 9d and e) the Al concentrations in solution do not change significantly with time.

Moreover, the change in Al concentrations over time is more distinct at lower NaOH concentrations compared to higher concentrations. In fact, for an increase in equilibration time from 3 months to 1 year the relative decrease in Al concentrations is higher for no alkali and 0.1 M NaOH, however, it is less in the presence of 0.5 M and 1 M NaOH. Since Al concentrations in solution are higher in the presence of higher NaOH concentrations (0.5 and 1 M), the changes in the concentrations over time are less visible. The measured concentrations of Al, Ca, Si and OH^- in solution are compiled in Supplementary Information B.

3.2.3. *The effect of equilibration time on Ca and Si concentrations in solution*

The results presented above, in particular, the decrease of secondary Al-containing phases with time and the decrease of Al concentrations in solution with time in the absence of secondary phases indicate the slow formation of thermodynamically more stable C-A-S-H phases with time. The effect of equilibration time on the concentrations of Ca and Si in solution at Ca/Si ratios of a) 0.8 and b) 1.2 is shown in Fig. 10 (data for the other Ca/Si ratios are shown in Supplementary Information E). The data measured at different Ca/Si ratios and at 0 to 0.1 Al/Si ratios are plotted as symbols as a function of pH and compared to the expected solubility of C-S-H indicated by lines. The measured values deviate to some extent from the modelled data, since the CSHQ model was developed based on data for alkali free C-S-H only [33,34] and needs to be further extended to describe the changes at high pH values and the uptake of alkalis in C-S-H as discussed in L'Hopital et al. [25].

In the absence of alkali hydroxide the Si and Ca concentrations do not vary significantly with time. At low Ca/Si ratios of 0.6 (Fig. E1 and 2 in Supplementary Information E) and 0.8 (Fig. 10a and b), no significant changes are observed in the Ca and Si concentrations in the absence of alkali hydroxide. The saturation indexes (SI) calculated from the measured concentrations indicate that the solution is near to saturation with respect to C-S-H in all cases. The solution is generally under saturated with respect to amorphous SiO_2 (with the exception of Ca/Si = 0.6 without NaOH), microcrystalline $Al(OH)_3$, katoite and strätlingite indicating that these phases will dissolve if precipitated initially. The SI values for different phases are presented in Supplementary Information C. At high alkali concentrations ($12 < pH < 14$), however, the Si concentrations slightly decrease in particular from 3 months to 1 year (Fig. 10b). Little variation with time is observed for Ca, with the exception of the outlier values after 1 year for Ca/Si = 0.8 at 0.1, 0.5 and 1 M NaOH, where might some contaminations prior to the Ca measurements had occurred). The observed changes in Si concentrations at high alkali concentrations can be associated to the disappearance of an unidentified calcium sodium aluminate silicate hydrate (C-N-A-S-H) phase with time, which is only observed at high alkali concentrations [25].

At high Ca/Si ratios of 1.0, 1.2 and 1.4 ($Ca/Si \geq 1.0$) the changes in Si and Ca concentrations in solution are small as shown in Fig. 10c and d (and Fig. E3–E6 in Supplementary Information E). At Ca/Si = 1.4 and high pH values, the Ca concentrations are also limited by the possible presence of portlandite.

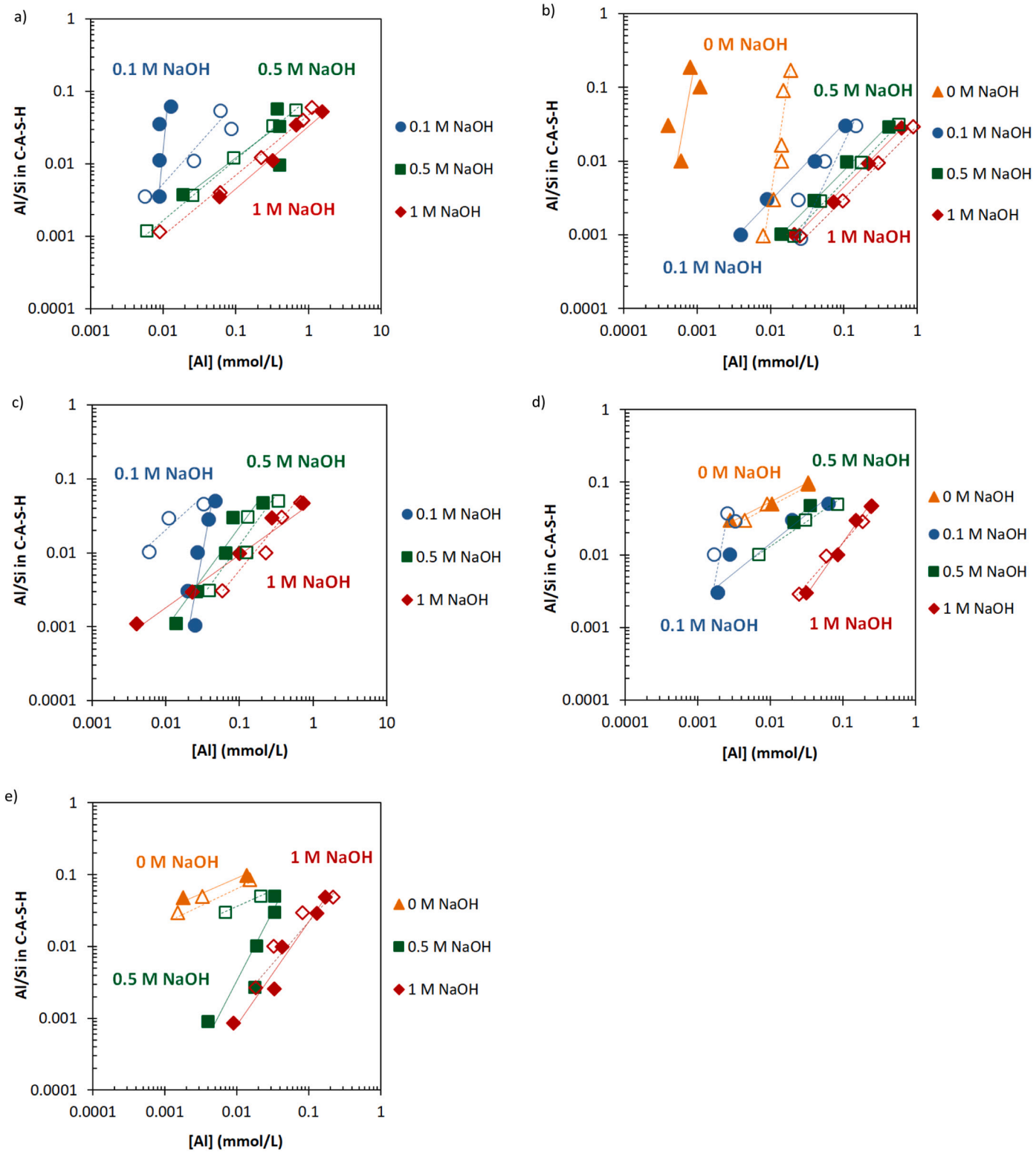

Fig. 9. The effect of equilibration time on Al uptake in C-S-H for Ca/Si ratios of a) 0.6; b) 0.8; c) 1.0; d) 1.2 and e) 1.4 at 0, 0.1, 0.5 and 1 M NaOH. The 3 months indicated by the empty and 1 year represented by the full symbols. The lines serve as eye-guides only.

3.2.4. The effect of equilibration time on C-A-S-H solubility

The solubility of C-A-S-H depends on the composition of the solid, i.e. the amount of Ca, Si and Al in the C-S-H structure, and is often described with solid solution models using different end-members [33,63,64]. The development of such solid solution models is generally based on a large number of experimental data and is a complex and challenging task, which is not within the focus of the present paper. However, the solubility of a single composition in equilibrium with the solution can easily be calculated based on the measured elemental concentrations.

The C-A-S-H solubility with Ca/Si ratios of 0.8 and 1.2 at Al/Si = 0.03 and 1 M NaOH is calculated as detailed in Eq. (3) and (4), assuming a constant composition of the solid C-A-S-H and is shown in Fig. 11 after

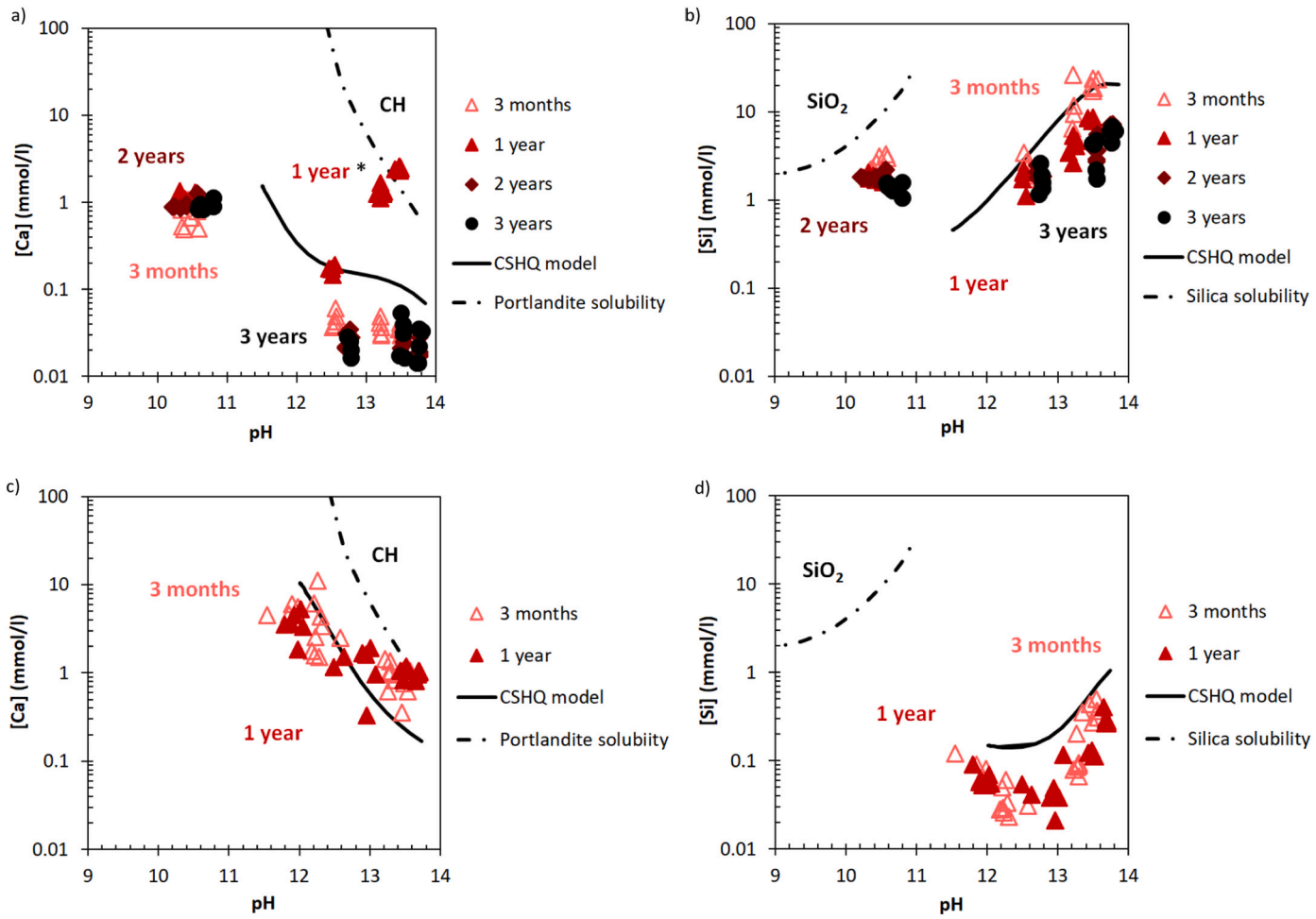

Fig. 10. The effect of pH and equilibration time on measured Ca (a,c) and Si (b,d) concentrations (symbols) and on the calculated solubility of C-S-H (using the CSHQ model [33]), portlandite and amorphous SiO_2 for Ca/Si ratios of a,b) 0.8 and c,d) 1.2 at 0, 0.1, 0.5 and 1 M NaOH (*: outlier Ca concentrations for Ca/Si = 0.8 after 1 year equilibration).

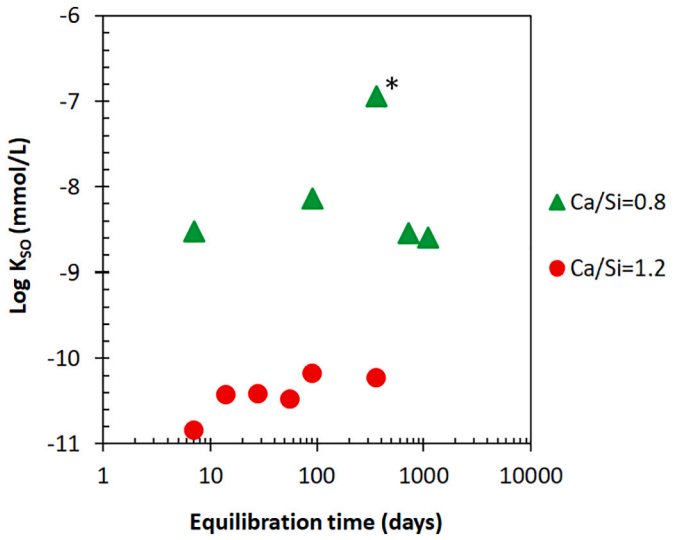

Fig. 11. The effect of equilibration time on C-A-S-H solubility product with Al/Si = 0.03 and 1 M NaOH. The Ca concentrations are below the detection limit (DL) for Ca/Si = 0.8 after 14, 28 and 56 days of equilibration. (*: higher value due to the outlier Ca concentrations for Ca/Si = 0.8 after 1 year equilibration).

different equilibration times. The solubility product of C-A-S-H with Ca/Si = 0.8 equals to $10^{-8.4\pm0.2}$ and does not change significantly with time indicating that the solubility is not dependent on the equilibration time. The observed decrease in Al concentrations with time due to its uptake in C-S-H is compensated by the small variations in Ca and Si concentrations. At Ca/Si = 1.2, a solubility product of $10^{-10.5\pm0.3}$ is observed with a tendency to increase from $10^{-10.8}$ to $10^{-10.2}$ from 7 days to 1 year. The derived values of the solubility products of $10^{-8.4\pm0.2}$ for Ca/Si = 0.8 and the somewhat lower values of $10^{-10.5\pm0.3}$ for Ca/Si = 1.2, agree well with the changes of the solubility products with Ca/Si ratio for C-S-H reported e.g. in [63]. The absence of any big changes in the solubility product with time despite the decrease in Al concentrations is an important result, which will help for the development of thermodynamic models for C-A-S-H.

4. Conclusions

The Al uptake in C-S-H was investigated after different equilibration times between 7 days to 3 years using sorption isotherm experiments. The experiments indicated that Al uptake in C-S-H increases with equilibration time and this change over time is more distinct at low Ca/Si ratios than at high Ca/Si ratios indicating that equilibrium is reached faster at high Ca/Si ratios. At low Ca/Si ratios, changes in Al and Si concentrations in solution were observed up to 3 years, although the changes were less important for the aged samples.

The solubility of C-A-S-H was calculated with thermodynamic

modeling using the concentrations measured after different equilibration times for C-A-S-H with Ca/Si ratios of 0.8 and 1.2. The calculation indicated that the solubility of C-A-S-H with Ca/Si = 0.8 and 1.2 does not change significantly with equilibration time.

In addition to the C-A-S-H phase, also secondary phases such as strätlingite, $Al(OH)_3$ and katoite formed initially, in particular at higher Al contents. Their content decreased in all cases after longer equilibration times indicating the dissolution of such secondary phases and an increase in uptake of Al in C-S-H. The FTIR analysis showed a restructuring of the C-A-S-H phase with time and this change is more significant at lower Ca/Si ratios.

CRediT authorship contribution statement

S. Barzgar: Methodology, Formal analysis, Investigation, Measurement, Modeling, Writing – Original Draft, Visualization,

M. Tarik: Formal analysis, Writing – Review & Editing, Supervision,

C. Ludwig: Formal analysis, Writing – Review & Editing, Supervision,

B. Lothenbach: Methodology, Formal analysis, Validation, Resources, Writing – Review & Editing, Supervision, Funding acquisition.

Declaration of competing interest

The authors declare that they have no known competing financial interests or personal relationships that could have appeared to influence the work reported in this paper.

Acknowledgments

The financial support of the Swiss National Science Foundation (SNF) [200021_169014] is gratefully acknowledged. The authors would like to thank Luigi Brunetti, Boris Ingold and Beatrice Fischer at Empa for support during the measurements.

Appendix A. Supplementary data

Supplementary data to this article can be found online at https://doi.org/10.1016/j.cemconres.2021.106438.

References

[1] R. Shahrin, C.P. Bobko, Characterizing strength and failure of calcium silicate hydrate aggregates in cement paste under micropillar compression, J. Nanomechanics Micromechanics. 7 (2017) 1–6, https://doi.org/10.1061/(ASCE)NM.2153-5477.0000137.

[2] P.J.M. Monteiro, S.A. Miller, A. Horvath, Towards sustainable concrete, Nat. Mater. 16 (2017) 698–699, https://doi.org/10.1038/nmat4930.

[3] B. Lothenbach, K. Scrivener, R.D. Hooton, Supplementary cementitious materials, Cem. Concr. Res. 41 (2011) 1244–1256, https://doi.org/10.1016/j.cemconres.2010.12.001.

[4] E. Gartner, Industrially interesting approaches to “low-CO2” cements, Cem. Concr. Res. 34 (2004) 1489–1498, https://doi.org/10.1016/j.cemconres.2004.01.021.

[5] M. Thomas, L. Barcelo, B. Blair, K. Cail, A. Delagrave, K. Kazanis, Lowering the carbon footprint of concrete by reducing clinker content of cement, Transp. Res. Rec. (2012) 99–104, https://doi.org/10.3141/2290-13.

[6] J. Li, W. Zhang, C. Li, P.J.M. Monteiro, Green concrete containing diatomaceous earth and limestone: workability, mechanical properties, and life-cycle assessment, J. Clean. Prod. 223 (2019) 662–679, https://doi.org/10.1016/j.jclepro.2019.03.077.

[7] E. L'Hôpital, B. Lothenbach, D.A. Kulik, K. Scrivener, Influence of calcium to silica ratio on aluminium uptake in calcium silicate hydrate, Cem. Concr. Res. 85 (2016) 111–121, https://doi.org/10.1016/j.cemconres.2016.01.014.

[8] L. Irbe, R.E. Beddoe, D. Heinz, The role of aluminium in C-A-S-H during sulfate attack on concrete, Cem. Concr. Res. 116 (2019) 71–80, https://doi.org/10.1016/j.cemconres.2018.11.012.

[9] S. Sakir, S.N. Raman, M. Safiuddin, A.B.M. Amrul Kaish, A.A. Mutalib, Utilization of by-products and wastes as supplementary cementitious materials in structural mortar for sustainable construction, Sustain. 12 (2020), https://doi.org/10.3390/su12093888.

[10] C. Ludwig, C.A. Johnson, M. Käppeli, A. Ulrich, S. Riediker, Hydrological and geochemical factors controlling the leaching of cemented MSWI air pollution control residues: a lysimeter field study, J. Contam. Hydrol. 42 (2000) 253–272, https://doi.org/10.1016/S0169-7722(99)00083-2.

[11] I. Baur, C. Ludwig, C. Annette Johnson, The leaching behavior of cement stabilized air pollution control residues: a comparison of field and laboratory investigations, Environ. Sci. Technol. 35 (2001) 2817–2822, https://doi.org/10.1021/es000243r.

[12] E. L'Hôpital, B. Lothenbach, G. Le Saout, D. Kulik, K. Scrivener, Incorporation of aluminium in calcium-silicate-hydrates, Cem. Concr. Res. 75 (2015) 91–103, https://doi.org/10.1016/j.cemconres.2015.04.007.

[13] R.J. Myers, S.A. Bernal, R. San Nicolas, J.L. Provis, Generalized structural description of calcium-sodium aluminosilicate hydrate gels: the cross-linked substituted tobermorite model, Langmuir. 29 (2013) 5294–5306, https://doi.org/10.1021/la4000473.

[14] G.L. Kalousek, Crystal chemistry of hydrous calcium silicates: I, substitution of aluminum in lattice of tobermorite, J. Am. Ceram. Soc. 40 (1957) 74–80.

[15] E. Bonaccorsi, S. Merlino, A.R. Kampf, The crystal structure of tobermorite 14 Å (plombierite), a C-S-H phase, J. Am. Ceram. Soc. 88 (2005) 505–512, https://doi.org/10.1111/j.1551-2916.2005.00116.x.

[16] J. Li, G. Geng, R. Myers, Y.S. Yu, D. Shapiro, C. Carraro, R. Maboudian, P.J.M. Monteiro, The chemistry and structure of calcium (alumino) silicate hydrate: a study by XANES, ptychographic imaging, and wide- and small-angle scattering, Cem. Concr. Res. 115 (2019) 367–378, https://doi.org/10.1016/j.cemconres.2018.09.008.

[17] S. Merlino, E. Bonaccorsi, T. Armbruster, Tobermorites: their real structure and order-disorder (OD) character, Am. Mineral. 84 (1999) 1613–1621, https://doi.org/10.2138/am-1999-1015.

[18] I.G. Richardson, A.R. Brough, R. Brydson, G.W. Groves, C.M. Dobson, Location of aluminium in substituted calcium silicate hydrate (C-S-H) gels as determined by Si-29 and Al-27 NMR and EELS, J. Am. Ceram. Soc. 76 (1993) 2285–2288, https://doi.org/10.1111/j.1151-2916.1993.tb07765.x.

[19] J. Li, G. Geng, W. Zhang, Y.S. Yu, D.A. Shapiro, P.J.M. Monteiro, The hydration of β- and α' H-dicalcium silicates: an X-ray spectromicroscopic study, ACS Sustain. Chem. Eng. 7 (2019) 2316–2326, https://doi.org/10.1021/acssuschemeng.8b05060.

[20] B. Lothenbach, A. Nonat, Calcium silicate hydrates: solid and liquid phase composition, Cem. Concr. Res. 78 (2015) 57–70, https://doi.org/10.1016/j.cemconres.2015.03.019.

[21] S. Ortaboy, J. Li, G. Geng, R.J. Myers, P.J.M. Monteiro, R. Maboudian, C. Carraro, Effects of CO2 and temperature on the structure and chemistry of C-(A-)S-H investigated by Raman spectroscopy, RSC Adv. 7 (2017) 48925–48933, https://doi.org/10.1039/c7ra07266j.

[22] J.J. Chen, J.J. Thomas, H.F.W. Taylor, H.M. Jennings, Solubility and structure of calcium silicate hydrate, Cem. Concr. Res. 34 (2004) 1499–1519, https://doi.org/10.1016/j.cemconres.2004.04.034.

[23] M.D. Andersen, H.J. Jakobsen, J. Skibsted, A new aluminium-hydrate species in hydrated Portland cements characterized by 27Al and 29Si MAS NMR spectroscopy, Cem. Concr. Res. 36 (2006) 3–17, https://doi.org/10.1016/j.cemconres.2005.04.010.

[24] A. Kunhi Mohamed, P. Moutzouri, P. Berruyer, B.J. Walder, J. Siramanont, J. Siramanont, M. Harris, M. Negroni, S.C. Galmarini, S.C. Parker, S.C. Parker, K. L. Scrivener, L. Emsley, P. Bowen, The atomic-level structure of cementitious calcium aluminate silicate hydrate, J. Am. Chem. Soc. 142 (2020) 11060–11071, https://doi.org/10.1021/jacs.0c02988.

[25] E.L. Hôpital, B. Lothenbach, K. Scrivener, D.A. Kulik, Alkali uptake in calcium alumina silicate hydrate (C-A-S-H), Cem. Concr. Res. 85 (2016) 122–136, https://doi.org/10.1016/j.cemconres.2016.03.009.

[26] X. Pardal, F. Brunet, T. Charpentier, I. Pochard, A. Nonat, 27Al and 29Si solid-state NMR characterization of calcium-aluminosilicate-hydrate, Inorg. Chem. 51 (2012) 1827–1836, https://doi.org/10.1021/ic202124x.

[27] X. Pardal, I. Pochard, A. Nonat, Experimental study of Si-Al substitution in calcium-silicate-hydrate (C-S-H) prepared under equilibrium conditions, Cem. Concr. Res. 39 (2009) 637–643, https://doi.org/10.1016/j.cemconres.2009.05.001.

[28] R.J. Myers, E. L'Hôpital, J.L. Provis, B. Lothenbach, Effect of temperature and aluminium on calcium (alumino)silicate hydrate chemistry under equilibrium conditions, Cem. Concr. Res. 68 (2015) 83–93, https://doi.org/10.1016/j.cemconres.2014.10.015.

[29] S. Barzgar, B. Lothenbach, M. Tarik, A. Di Giacomo, C. Ludwig, The effect of sodium hydroxide on Al uptake by calcium silicate hydrates (C-S-H), J. Colloid Interface Sci. 572 (2020) 246–256, https://doi.org/10.1016/j.jcis.2020.03.057.

[30] B. Traynor, H. Uvegi, E. Olivetti, B. Lothenbach, R.J. Myers, Methodology for pH measurement in high alkali cementitious systems, Cem. Concr. Res. 135 (2020) 106122, https://doi.org/10.1016/j.cemconres.2020.106122.

[31] B. Lothenbach, P. Durdziński, K. De Weerdt, Thermogravimetric analysis (TGA), in: A Pract. Guid. to Microstruct. Anal. Cem. Mater., 1st ed., CRC Press, 2016, pp. 178–208, https://doi.org/10.1201/b19074-5.

[32] E. Bernard, B. Lothenbach, D. Rentsch, I. Pochard, A. Dauzères, Formation of magnesium silicate hydrates (M-S-H), Phys. Chem. Earth 99 (2017) 142–157, https://doi.org/10.1016/j.pce.2017.02.005.

[33] D.A. Kulik, Improving the structural consistency of C-S-H solid solution thermodynamic models, Cem. Concr. Res. 41 (2011) 477–495, https://doi.org/10.1016/j.cemconres.2011.01.012.

[34] T. Wagner, D.A. Kulik, F.F. Hingerl, S.V. Dmytrievava, Gem-selektor geochemical modeling package: TSolMod library and data interface for multicomponent phase models, Can. Mineral. 50 (2012) 1173–1195, https://doi.org/10.3749/canmin.50.5.1173.

[35] T. Thoenen, W. Hummel, U. Berner, E. Curti, The PSI/Nagra Chemical Thermodynamic Database 12/07, Villigen PSI, 2014. https://www.psi.ch/sites/default/files/import/les/DatabaseEN/PSI-Bericht%252014-04_final_druckerei.pdf.

[36] B. Lothenbach, D.A. Kulik, T. Matschei, M. Balonis, L. Baquerizo, B. Dilnesa, G. D. Miron, R.J. Myers, Cemdata18: a chemical thermodynamic database for hydrated Portland cements and alkali-activated materials, Cem. Concr. Res. 115 (2019) 472–506, https://doi.org/10.1016/j.cemconres.2018.04.018.
[37] B. Ma, B. Lothenbach, Thermodynamic study of cement/rock interactions using experimentally generated solubility data of zeolites, Cem. Concr. Res. 135 (2020) 106–149, https://doi.org/10.1016/j.cemconres.2020.106149.
[38] H.C. Helgeson, D.H. Kirkham, G.G. Flowers, Theoretical prediction of the thermodynamic behavior of aqueous electrolytes at high pressure and temperature: IV. Calculation of activity coefficients, osmotic coefficients, and apparent molal and standard and relative partial molal properties to 600°C a, Am. J. Sci. 281 (1981) 1249–1516.
[39] B.J. Merkel, B. Planer-friedrich, Groundwater Geochemistry: A Practical Guide to Modeling of Natural and Contaminated Aquatic Systems, 2nd ed., Springer, Berlin, 2008 https://doi.org/10.1007/b138774.
[40] A.C.A. Muller, K.L. Scrivener, A.M. Gajewicz, P.J. McDonald, Use of bench-top NMR to measure the density, composition and desorption isotherm of C-S-H in cement paste, Microporous Mesoporous Mater. 178 (2013) 99–103, https://doi.org/10.1016/j.micromeso.2013.01.032.
[41] P. Suwanmaneechot, A. Aili, I. Maruyama, Creep behavior of C-S-H under different drying relative humidities: interpretation of microindentation tests and sorption measurements by multi-scale analysis, Cem. Concr. Res. 132 (2020) 106036, https://doi.org/10.1016/j.cemconres.2020.106036.
[42] E. Kapeluszna, Ł. Kotwica, A. Różycka, Ł. Gołek, Incorporation of Al in C-A-S-H gels with various Ca/Si and Al/Si ratio: microstructural and structural characteristics with DTA/TG, XRD, FTIR and TEM analysis, Constr. Build. Mater. 155 (2017) 643–653, https://doi.org/10.1016/j.conbuildmat.2017.08.091.
[43] A. Adamczyk, E. Długoń, The FTIR studies of gels and thin films of Al2O3-TiO2 and Al2O3-TiO2-SiO2 systems, Spectrochim. Acta - Part A Mol. Biomol. Spectrosc. 89 (2012) 11–17, https://doi.org/10.1016/j.saa.2011.12.018.
[44] W. Mozgawa, M. Król, T. Bajda, IR spectra in the studies of anion sorption on natural sorbents, J. Mol. Struct. 993 (2011) 109–114, https://doi.org/10.1016/j.molstruc.2010.11.070.
[45] C.A. Ríos, C.D. Williams, M.A. Fullen, Hydrothermal synthesis of hydrogarnet and tobermorite at 175 °C from kaolinite and metakaolinite in the CaO-Al2O3-SiO2-H2O system: a comparative study, Appl. Clay Sci. 43 (2009) 228–237, https://doi.org/10.1016/j.clay.2008.09.014.
[46] S. Wang, X. Peng, L. Tang, L. Zeng, C. Lan, Influence of inorganic admixtures on the 11 Å-tobermorite formation prepared from steel slags: XRD and FTIR analysis, Constr. Build. Mater. 60 (2014) 42–47, https://doi.org/10.1016/j.conbuildmat.2014.03.002.
[47] N.Y. Mostafa, A.A. Shaltout, H. Omar, S.A. Abo-El-Enein, Hydrothermal synthesis and characterization of aluminium and sulfate substituted 1.1 nm tobermorites, J. Alloys Compd. 467 (2009) 332–337, https://doi.org/10.1016/j.jallcom.2007.11.130.
[48] H. Maeda, E.H. Ishida, T. Kasuga, Hydrothermal preparation of tobermorite incorporating phosphate species, Mater. Lett. 68 (2012) 382–384, https://doi.org/10.1016/j.matlet.2011.11.017.
[49] E.I. Al-Wakeel, S.A. El-Korashy, Reaction mechanism of the hydrothermally treated CaO-SiO2-Al2O3 and CaO-SiO2-Al2O3-CaSO4 systems, J. Mater. Sci. 31 (1996) 1909–1913, https://doi.org/10.1007/BF00372207.
[50] P. Yu, R.J. Kirkpatrick, B. Poe, P.F. McMillan, X. Cong, Structure of calcium silicate hydrate (C-S-H): near-, mid-, and far-infrared spectroscopy, 82 (1999) 742–748.
[51] J. Higl, D. Hinder, C. Rathgeber, B. Ramming, M. Lindén, Detailed in situ ATR-FTIR spectroscopy study of the early stages of C-S-H formation during hydration of monoclinic C3S, Cem. Concr. Res. 142 (2021) 106367, https://doi.org/10.1016/j.cemconres.2021.106367.
[52] L. Fernandez, C. Alonso, A. Hidalgo, C. Andrade, The role of magnesium during the hydration of C3S and C-S-H formation. Scanning electron microscopy and mid-infrared studies, Adv. Cem. Res. 17 (2005) 9–21, https://doi.org/10.1680/adcr.2005.17.1.9.
[53] L. Fernández-Carrasco, D. Torrens-Martín, L.M. Morales, S. Martínez-Ramírez, Infrared spectroscopy in the analysis of building and construction materials, in: Infrared Spectrosc. - Mater. Sci. Eng. Technol., Intech, 2012, pp. 369–382, https://doi.org/10.5772/36186.
[54] P. Padmaja, G.M. Anilkumar, P. Mukundan, G. Aruldhas, K.G.K. Warrier, Characterisation of stoichiometric sol-gel mullite by fourier transform infrared spectroscopy, Int. J. Inorg. Mater. 3 (2001) 693–698, https://doi.org/10.1016/S1466-6049(01)00189-1.
[55] J. Partyka, M. Leśniak, Raman and infrared spectroscopy study on structure and microstructure of glass-ceramic materials from SiO_2-Al_2O_3-Na_2O-K_2O-CaO system modified by variable molar ratio of SiO_2/Al_2O_3, Spectrochim. Acta - Part A Mol. Biomol. Spectrosc. 152 (2016) 82–91, https://doi.org/10.1016/j.saa.2015.07.045.
[58] K. Djebaili, Z. Mekhalif, A. Boumaza, A. Djelloul, XPS, FTIR, EDX, XRD analysis of Al_2O_3 scales grown on Pm2000 alloy, J. Spectrosc. 2015 (2015) 1–16, https://doi.org/10.1155/2015/868109.
[59] C. Liu, K. Shih, Y. Gao, F. Li, L. Wei, Dechlorinating transformation of propachlor through nucleophilic substitution by dithionite on the surface of alumina, J. Soils Sediments 12 (2012) 724–733, https://doi.org/10.1007/s11368-012-0506-0.
[60] S. Vasudevan, B.S. Kannan, J. Lakshmi, S. Mohanraj, G. Sozhan, Effects of alternating and direct current in electrocoagulation process on the removal of fluoride from water, J. Chem. Technol. Biotechnol. 86 (2011) 428–436, https://doi.org/10.1002/jctb.2534.
[61] N. Garg, V.O. Özçelik, J. Skibsted, C.E. White, Nanoscale ordering and Depolymerization of calcium silicate hydrates in the presence of alkalis, J. Phys. Chem. C 123 (2019) 24873–24883, https://doi.org/10.1021/acs.jpcc.9b06412.
[62] N.V. Chukanov, Infrared Spectra of Mineral Species, Springer Netherlands, http://link.springer.com/10.1007/978-94-007-7128-4, 2014.
[63] C.S. Walker, S. Sutou, C. Oda, M. Mihara, A. Honda, Calcium silicate hydrate (C-S-H) gel solubility data and a discrete solid phase model at 25 °C based on two binary non-ideal solid solutions, Cem. Concr. Res. 79 (2016) 1–30, https://doi.org/10.1016/j.cemconres.2015.07.006.
[64] R.J. Myers, S.A. Bernal, J.L. Provis, A thermodynamic model for C-(N-)A-S-H gel: CNASH-ss. Derivation and validation, Cem. Concr. Res. 66 (2014) 27–47, https://doi.org/10.1016/j.cemconres.2014.07.005.